

RESEARCH ARTICLE

10.1002/2016JD024955

Key Points:

- Our model simulation suggests that both the temporal and spatial slopes remain largely stable throughout the last deglaciation
- On average, the temporal slope (around 0.3) is about half of the spatial slope
- The smaller temporal slope in extratropics is mainly because of the polar amplification feature in global climate change

Supporting Information:

- Supporting Information S1

Correspondence to:

J. Guan and Z. Liu,
lotusescy@pku.edu.cn;
zliu3@wisc.edu

Citation:

Guan, J., Z. Liu, X. Wen, E. Brady, D. Noone, J. Zhu, and J. Han (2016), Understanding the temporal slope of the temperature-water isotope relation during the deglaciation using isoCAM3: The slope equation, *J. Geophys. Res. Atmos.*, 121, doi:10.1002/2016JD024955.

Received 17 FEB 2016

Accepted 2 AUG 2016

Accepted article online 4 AUG 2016

Understanding the temporal slope of the temperature-water isotope relation during the deglaciation using isoCAM3: The slope equation

Jian Guan¹, Zhengyu Liu², Xinyu Wen¹, Esther Brady³, David Noone⁴, Jiang Zhu², and Jing Han¹

¹Laboratory for Climate, Ocean and Atmosphere Studies, Department of Atmospheric and Oceanic Sciences, School of Physics, Peking University, Beijing, China, ²Department Atmospheric and Oceanic Sciences and Center for Climate Research/Nelson Institute for Environmental Studies, University of Wisconsin-Madison, Madison, Wisconsin, USA, ³Climate and Global Dynamics, Earth System Laboratory, NCAR, Boulder, Colorado, USA, ⁴College of Earth, Ocean and Atmospheric Sciences, Oregon State University, Corvallis, Oregon, USA

Abstract The temporal and spatial slopes of water isotope-temperature relations are studied for the last 21,000 years over the middle and high latitudes using a series of snapshot simulations of global climate and water isotopes in the isotope-enabled atmospheric model isoCAM3. Our model simulation suggests that both the temporal slope and spatial slope remain largely stable throughout the last deglaciation. Furthermore, the temporal slope can vary substantially across regions. Nevertheless, on average, and most likely, the temporal slope is about $0.3\text{‰}\text{°C}^{-1}$ and is about half of the spatial slope. Finally, the relation between temporal and spatial slopes is understood using a semiempirical equation that is derived based on both the Rayleigh distillation and a fixed spatial slope. The slope equation quantifies the Boyle's mechanism and suggests that the temporal slope is usually smaller than the spatial slope in the extratropics mainly because of the polar amplification feature in global climate change, such that the response in local temperature at middle and high latitudes is usually greater than that in the total equivalent source temperature.

1. Introduction

Water stable isotopologues (hereafter isotope) in precipitation has been suggested to provide an effective indicator of the surface air temperature (SAT) changes in the middle and high latitudes due to the so-called temperature effect [Dansgaard, 1964]. Present-day observations in the middle and high latitudes show a highly significant spatial correlation between the annual mean SAT and precipitation $\delta^{18}\text{O}$ ($\delta^{18}\text{O} = \frac{(^{18}\text{O}/^{16}\text{O})_{\text{sample}} - (^{18}\text{O}/^{16}\text{O})_{\text{SMOW}}}{(^{18}\text{O}/^{16}\text{O})_{\text{SMOW}}} \cdot 10^3\text{‰}$, SMOW = Standard Mean Ocean Water [Craig, 1961]) with a regression coefficient (spatial slope) of $0.69\text{‰}\text{°C}^{-1}$ [Dansgaard, 1964]. This present-day spatial slope was then used to infer the temporal evolution of temperature changes particularly for polar regions [e.g., Grootes et al., 1993] as if it can serve as an analogue for temporal relationship (temporal slope). This inference requires two key assumptions: the spatial slopes remain unchanged over time, and the value of the spatial slope is similar to the temporal slope in the past.

The validity of the two assumptions above, however, has been challenged by other reconstructions such as borehole paleothermometry [Cuffey et al., 1994, 1995; Johansen et al., 1995] and nitrogen isotopes [Buizert et al., 2014], as well as isotope-enabled numerical simulations [e.g., Liu et al., 2012]. For example, borehole temperature reconstruction over Greenland showed a warming $\sim 23 \pm 2\text{°C}$ from the Last Glacial Maximum (LGM) to the present, inferring a temporal slope $0.35\text{‰}\text{°C}^{-1}$, which is about half of the present spatial slope [Cuffey et al., 1995; Jouzel et al., 1997]. A similar discrepancy also exists in the Antarctica, for example, in the Vostok ice core [Salamatin et al., 1998], although later work [Jouzel et al., 2003] indicates that the present-day spatial slope can be used as an analogue of the temporal slope to interpret the temperature changes during the glacial-interglacial cycle at the Vostok and European Project for Ice Coring in Antarctica (EPICA) Dome C sites within an error of $\sim 10\text{--}30\%$.

The reduced temporal slope relative to the spatial slope has been examined in both observational and modeling studies. Assuming a fixed spatial slope from the LGM to the Holocene and using a graphic

technique, Boyle [1997] interpreted the reduced temporal slope of $0.35\text{‰}\text{°C}^{-1}$ in terms of a $\sim 5\text{°C}$ tropical sea surface temperature (SST) cooling in the source region and a 1‰ global enrichment associated with the reduction of ice volume. Hendricks *et al.* [2000] argues that the distillation effect is not dominant before reaching the midlatitudes because of the large evaporative recharge occurring in the subtropics. They indicate that the critical latitude between the evaporation-dominated zone and distillation zone is about 45°S in the Southern Hemisphere. Several studies also show that the local source region has a non-negligible contribution to the total amount of precipitation over Greenland [Werner *et al.*, 2001; Sodemann *et al.*, 2008].

Atmospheric general circulation model (AGCM) simulations suggested that the change of precipitation seasonality at the LGM can lead to a warmer LGM bias in the reconstructions of temperature than implied from the spatial slope [Krinner *et al.*, 1997; Werner *et al.*, 2000]. Lee *et al.* [2008] argue that the change of precipitation seasonality can only partly explain the difference between spatial and temporal slopes. They further suggested that the evaporative recharge over the Southern Ocean can reduce the $\delta^{18}\text{O}$ difference in water vapor between LGM and present and, in turn, reduce the temporal slope near the edge of the sea ice ($\sim 60\text{°S}$), and this reduction effect weakens inland (also shown in Hendricks *et al.* [2000]).

Most past studies on the temporal and spatial slopes, especially those modeling studies, have focused on two regions, Greenland and Antarctica, and two climate states: LGM and present. This has left several questions wide open. First, has the temporal and spatial slope changed significantly over the deglaciation? Second, what are the temporal slopes in other regions of the world? Finally, what is the mechanism that determines the temporal slope in the middle and high latitudes regionally and globally? Here we will address these questions with a series of “time slice” experiments of water isotopes and climate of the last 21,000 years [Liu *et al.*, 2014] in an isotope-enabled AGCM isoCAM3 which incorporates fractionation associated with moisture convection and cloud processes and surface evaporation [Noone and Sturm, 2010]. Our modeling study shows that over the middle and high latitudes, the spatial slope has remained relatively stable in the last 21,000 years with a mean of $\sim 0.6\text{‰}\text{°C}^{-1}$, while the temporal slope can vary substantially among different regions. However, overall, the temporal slope is about half of the spatial slope. Furthermore, a semiempirical slope equation is developed based on Rayleigh distillation and a fixed spatial slope. The slope equation sets the Boyle’s interpretation in a more quantitative framework. As such, the reduced temporal slope relative to spatial slope can be interpreted, approximately, as caused by a greater change in local temperature than source temperature or polar amplification.

The paper is arranged as follows. Section 2 will describe the observational data and model experiments and compare the isotope-temperature relation between the data and model for present day. Section 3 will describe the spatial and temporal isotope-temperature relationship in our simulations. Section 4 will discuss the mechanism of the temporal slope in terms of a semiempirical equation for the ratio between temporal and spatial slopes. Finally, in section 5, we summarize the results and further discuss the potential mechanism that can affect the difference between temporal and spatial relationships.

2. Data and Model Experiments

We first discuss the model simulation climate and water isotope distribution of the present, in comparison with observations. In this study, the spatial and temporal slopes are discussed mainly in terms of the annual mean precipitation weighted oxygen isotope (hereafter $\delta^{18}\text{O}_w$) and the annual mean SAT (without precipitation weighting). The observational data on water isotopes used in this study is from the Global Network of Isotopes in Precipitation (GNIP) since 1961 for the stations where both the monthly mean isotope record and meteorological data (i.e., temperature and precipitation) are available.

The model output is from 23 snapshot simulations of the last 22,000 years simulated using the isotope-enabled atmospheric component model of the National Center for Atmospheric Research Community Climate System Model version 3, isoCAM3 [Noone and Sturm, 2010; Liu *et al.*, 2014] with the resolution of T31 (which is the equivalent of a horizontal resolution of $3.75\text{°}\times 3.75\text{°}$). The 23 experiments are 1000 years apart from each other, at 22 ka, 21 ka, ..., 00 ka. Each experiment is forced by the realistic external forcing of solar insolation, atmospheric greenhouse gases, and continental ice sheets, the same as for the Transient simulation of Climate Evolution (TraCE) experiment in Liu *et al.* [2009], and, in addition, by a 50 year history

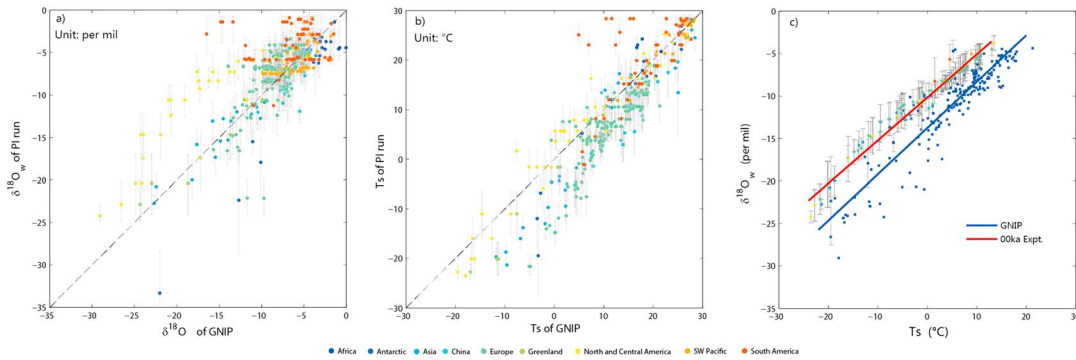


Figure 1. Comparison between the present (00 ka) experiment and GNIP records at the same location. (a) The annual mean $\delta^{18}\text{O}_w$ in 00 ka experiment against the GNIP records; (b) the annual mean T_s in 00 ka experiment against the GNIP records; (c) spatial relationship over extratropical regions (40°N – 90°N and 45°S – 90°S) between the annual mean SAT and annual mean $\delta^{18}\text{O}_w$ (weighted by precipitation) in GNIP (blue) and 00 ka experiment (red). The modeled data are plotted as the average of the values of the nine nearby grid boxes (the center grid box containing the data point and the eight surrounding grid boxes). The grey bars represent the spatial standard deviation in the model. The spatial slope calculated with the model data is $0.51\text{‰}\text{C}^{-1}$, which is close to the GNIP result ($0.54\text{‰}\text{C}^{-1}$).

of interannually varying monthly sea surface temperature (SST) and sea ice cover from TRACE. Surface ocean $\delta^{18}\text{O}$ values are changed from 1.6‰ at LGM (22 ka) [Schrag *et al.*, 1996] to 0.5‰ at present (0 ka) following the sea level changes. The monthly mean of the last 30 years of each snapshot is used for analysis in this study.

The model largely reproduces the major features of the present-day isotope-temperature relationship. The annual mean $\delta^{18}\text{O}_w$ (Figure 1a) and annual mean SAT (Figure 1b) in the present (00 ka) experiment are compared with the GNIP records at the same location. Qualitatively, the model results show better agreement with the observation in the annual mean SAT (r^2 is 0.81) than that of annual mean $\delta^{18}\text{O}_w$ (r^2 is 0.62). For convenience of discussion, the GNIP observations are divided into nine groups according to the geographic location (Table 1), with each group marked by different colors in Figures 1a and 1b. The model produces water isotopes too enriched in the North and Central America and too depleted in South Africa and Antarctica (Figure 1a) compared with GNIP, yet it reproduces the spatial gradient of the water isotope signals and SAT well. Quantitatively, the extratropical spatial slope in both hemispheres in the 00 ka experiment is $\sim 0.50\text{‰}\text{C}^{-1}$, similar to the spatial slope from the GNIP records ($\sim 0.54\text{‰}\text{C}^{-1}$) (Figure 1c). For the northern extratropics, the spatial slope of GNIP records ($\sim 0.56\text{‰}\text{C}^{-1}$) is captured by the model, while for the southern extratropics, the spatial slope in GNIP ($\sim 0.46\text{‰}\text{C}^{-1}$) is smaller than in the model by $\sim 0.15\text{‰}\text{C}^{-1}$. In addition, for interannual variability, the averaged temporal slope between annual mean SAT and annual mean $\delta^{18}\text{O}_w$ over Greenland in 00 ka experiment is $\sim 0.31\text{‰}\text{C}^{-1}$, also comparable with that from the contemporaneous observations there (North Greenland: $\sim 0.28\text{‰}\text{C}^{-1}$ in Shuman *et al.* [2001]). Overall, the isotope-temperature relation in the model is reasonably consistent with the observation.

Table 1. The GNIP Records Are Divided Into Nine Groups According to Their Geographic Location, About Half of Which Are Available

Region	Station Number (Available/All)
Africa	22/114
Antarctic	4/4
Asia	52/127
China ^a	20/33
Europe	191/400
Greenland ^a	6/7
North and Central America	49/108
Southwest Pacific	56/80
South America	64/171
Total	438/1004

^aGroup China and Greenland are included in Asia and Europe, respectively.

3. Spatial and Temporal Slopes

Now we compare the temporal slope during the deglaciation with the spatial slope in the model. We will focus on the extratropics, 40°N – 90°N in the Northern Hemisphere and 45°S – 90°S in the Southern Hemisphere, where the isotope-temperature relationship is dominated by the temperature effect. Unlike in previous modeling studies, we will examine the changes of the temporal and spatial slopes from both the regional and global perspectives. Therefore, we will examine the temporal

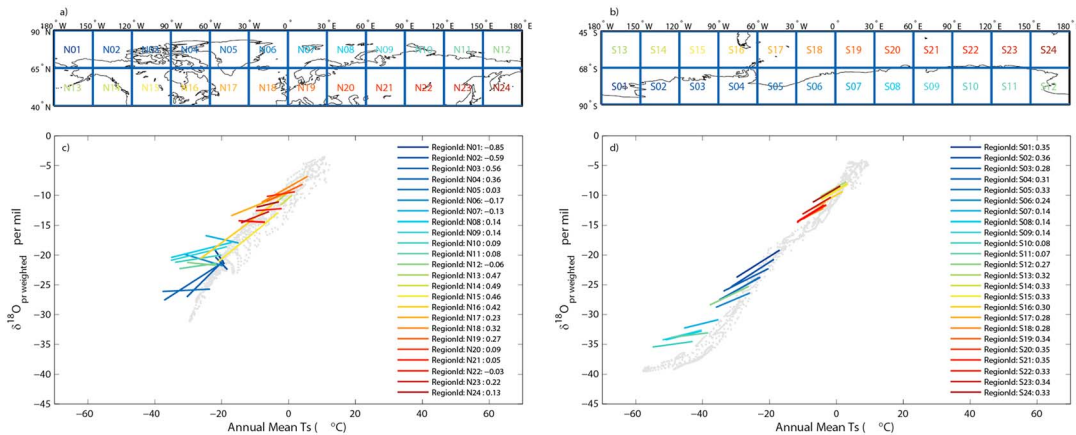


Figure 2. Annual mean SAT- $\delta^{18}O_w$ spatial relationship (grey) in the extratropics where the temperature effect is dominant (NH, left; SH, right) in the 00 ka experiment. (a, b) The extratropics in each hemisphere is divided into 24 subregions, with each subregion about 30° in longitude and $12\text{--}15^\circ$ in latitude. (c, d) Each line represents the temporal regressions across the 23 snapshots between the area-averaged annual mean SAT and $\delta^{18}O_w$ in one subregion. The length of each line shows the regional-averaged annual mean SAT and $\delta^{18}O_w$ changes from the LGM to present. The legend gives the temporal slope value of each region with its corresponding color.

and spatial slopes across the extratropics in both hemispheres. The extratropics is divided into 24 subregions in each hemisphere as shown in Figure 2, with each subregion about 30° in longitude and $12\text{--}15^\circ$ in latitude, containing about 48 grid boxes.

First, in each subregion or averaged over each hemisphere, the spatial slope does not change substantially from LGM (Northern Hemisphere (NH), $0.49\text{‰}\text{ }^\circ\text{C}^{-1}$; Southern Hemisphere (SH), $0.50\text{‰}\text{ }^\circ\text{C}^{-1}$) to the present (NH, $0.55\text{‰}\text{ }^\circ\text{C}^{-1}$; SH, $0.63\text{‰}\text{ }^\circ\text{C}^{-1}$). This can be seen in Figure 3 (top and bottom) for the evolution of the area-weighted spatial slopes averaged in the two hemispheres. The largest change occurs in the northern polar region ($67^\circ\text{N}\text{--}90^\circ\text{N}$), with an increasing trend from $\sim 0.5\text{‰}\text{ }^\circ\text{C}^{-1}$ at LGM to $0.7\text{‰}\text{ }^\circ\text{C}^{-1}$ at the present. Over Greenland, the local spatial slope shows a small increasing trend from $\sim 0.6\text{‰}\text{ }^\circ\text{C}^{-1}$ at the LGM to $\sim 0.8\text{‰}\text{ }^\circ\text{C}^{-1}$ at the present.

Second, the temporal slope is usually smaller than the spatial slope. This can be seen in Figures 2c and 2d for the extratropical Northern and Southern Hemispheres, respectively. In each hemisphere, the spatial slope can be inferred from the relation between annual mean $\delta^{18}O_w$ and SAT (00 ka experiment, in grey dots). (Note, as discussed in Figure 3, that the spatial slope remains largely unchanged at other time slices.) The temporal slope for each subregion is calculated as the regression coefficient between the area-weighted annual mean $\delta^{18}O_w$ and the annual mean SAT across the 23 snapshots and is plotted as a straight line with the slope as the temporal slope. The length of each line represents the ranges of the $\delta^{18}O_w$ (along x axis) and SAT (along y axis) changes in the last 21,000 years in each subregion, with the right end point plotted at the $\delta^{18}O_w$ and SAT values of the 00 ka experiment. For example, for the N18 region, the line starts from its present-day $\delta^{18}O_w \sim -7\text{‰}$ and SAT $\sim 5^\circ\text{C}$ (right/upmost point), with the minimum at the points of $\delta^{18}O_w \sim -12\text{‰}$ and SAT $\sim -10^\circ\text{C}$ (at LGM), connected with an orange straight line of the temporal slope of $\sim 0.32\text{‰}\text{ }^\circ\text{C}^{-1}$. The most striking feature in Figures 2c and 2d is that for most subregions, the temporal slope is positive and the magnitude is smaller than the spatial slope. In the mean time, there are also substantial differences in the temporal slopes, in particular, in a few regions north of Alaska (N01 and N02), where the temporal slope becomes negative. These negative slopes appear to be caused by the topographic effect of the Cordilleran ice sheet on the circulation [e.g., Lofverstrom et al., 2014] and in turn temperature and water isotopes, a point to be returned to later.

As a further comparison of the spatial and temporal slopes, we plot the histogram of the spatial and temporal slopes of all the subregions in the NH in Figures 4a and 4b, respectively. For both slopes, the robustness is measured by the square of the correlation (R^2), plotted as a dot on the left. Most of the spatial and temporal slopes pass the 95% significance T test ($R^2 > 0.10$ for spatial slopes and $R^2 > 0.17$ for temporal slopes). A comparison of the histograms of temporal and spatial slopes show clearly an overall smaller temporal slope. The average spatial slope (with high explained variance $R^2 > 0.36$) are $\sim 0.54\text{‰}\text{ }^\circ\text{C}^{-1}$ in the Northern

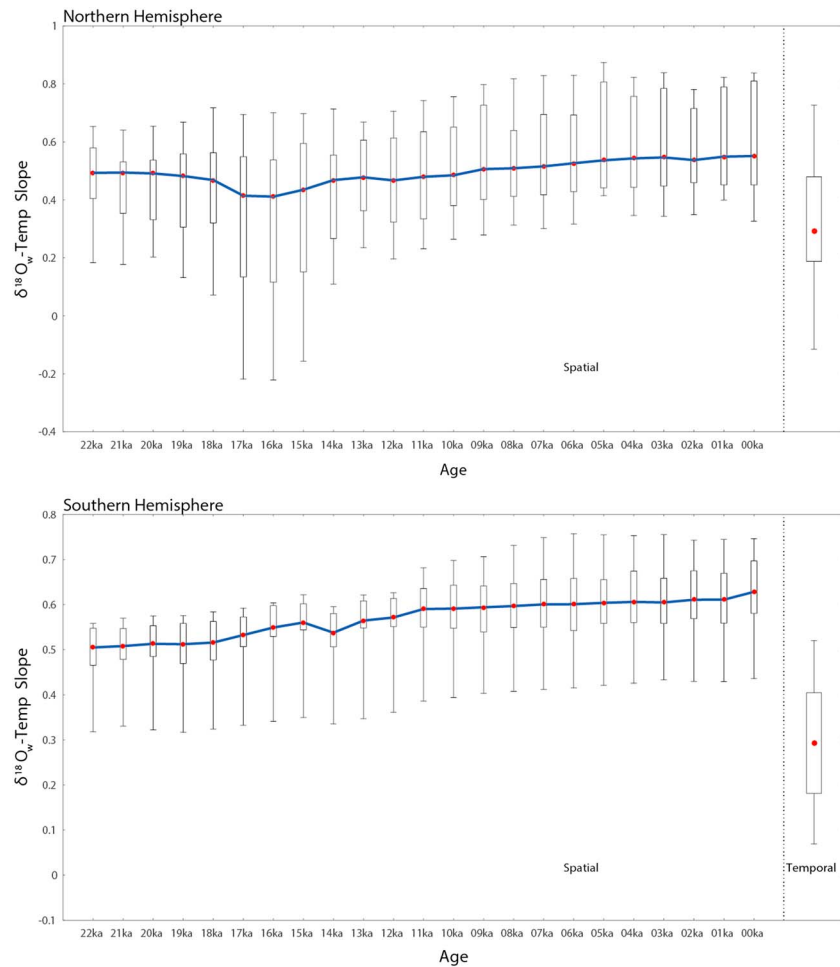


Figure 3. The evolution of (left) the spatial slope and (right) the temporal slope for 24 subregions in (a) Northern and (b) Southern Hemispheres. For a single experiment like 00 ka, the box shows the range from the 25th percentile to 75th percentile. The bottom line represents the 10th percentile, and the top line represents the 90th percentile. The red dot represents the mean value of spatial (area-weighted) or temporal slope.

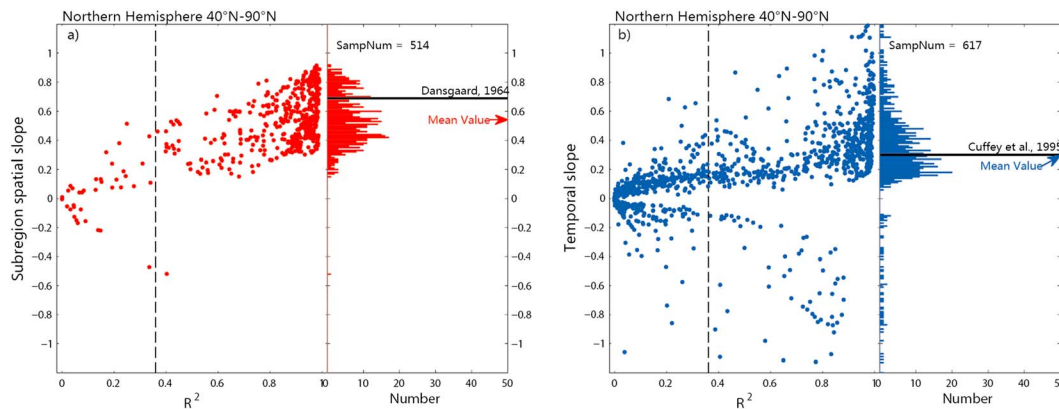


Figure 4. The scatterplot and frequency statistics plot of (a) the spatial (red) and (b) temporal (blue) slope of extratropics in the Northern Hemisphere. The spatial slope and the corresponding explained variance (R^2) is calculated by each separated region's ($N_1, N_2, N_3, \dots, N_{24}$) annual mean SAT and $\delta^{18}O_w$ for all snapshots simulations (The 95% significance level is 0.10). The temporal slope and the corresponding explained variance (R^2) is calculated by annual mean SAT and $\delta^{18}O_w$ of all grids in each subregion (The 95% significance level is 0.17). The histogram plot is the frequency statistics for the slope whose R^2 is larger than 0.36. The mean spatial slope is $0.54\% \text{ } ^\circ\text{C}^{-1}$, slightly smaller than the present observation of $0.69\% \text{ } ^\circ\text{C}^{-1}$ [Dansgaard, 1964], and the average temporal slope is $0.29\% \text{ } ^\circ\text{C}^{-1}$, close to the borehole estimation of $0.3\% \text{ } ^\circ\text{C}^{-1}$ [cp, 1995].

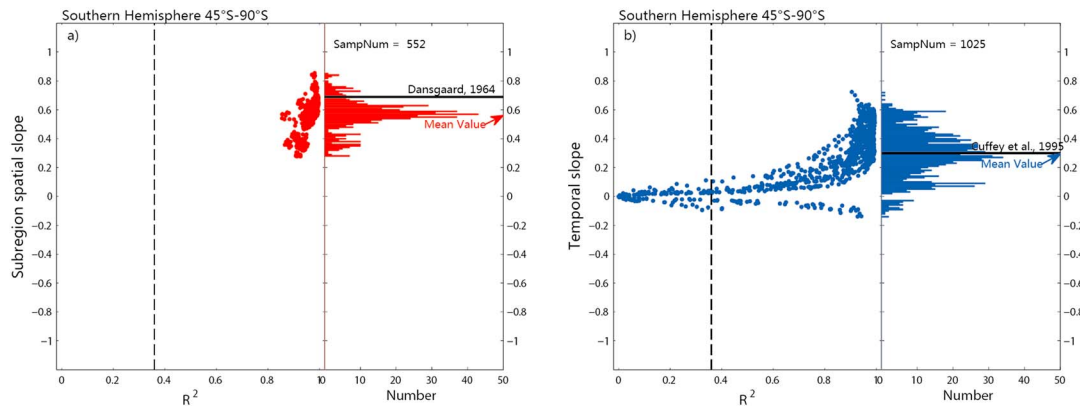


Figure 5. The same plot as Figure 4 but for middle and high latitudes in the Southern Hemisphere. The average spatial and temporal slopes in the Southern Hemisphere are $0.56‰\text{ }^{\circ}\text{C}^{-1}$ and $0.29‰\text{ }^{\circ}\text{C}^{-1}$, respectively.

Hemisphere. In contrast, the temporal slope is $\sim 0.29‰\text{ }^{\circ}\text{C}^{-1}$. The overall reduced temporal slope relative to spatial slope during the entire deglaciation can also be seen in Figure 3 (top), where the time evolution of the spatial slope can be compared with the temporal slope plotted on the right-hand side. Therefore, on average, the temporal slope is about a half of the spatial slope in the model in the NH. This conclusion also holds for the SH, as seen in the spatial and temporal slopes in Figures 5a and 5b, respectively, and the evolution of spatial slope in Figure 3 (bottom).

It is interesting that the averaged model temporal slopes in both the NH and SH are almost identical to the observed temporal slope over Greenland in terms of the borehole paleothermometry and Greenland ice cores $\delta^{18}\text{O}_w$ ($0.30‰\text{ }^{\circ}\text{C}^{-1}$ [Cuffey et al., 1995; Johnsen et al., 1997]). In contrast, the model temporal slope locally over Greenland is much suppressed (subregion N05 in Figure 2a) than in the ice core observations. Similarly, the model temporal slope in the Antarctica, e.g., in EPICA Dome C (S11 in Figure 2b) is also suppressed severely compared with the ice core observation [Jouzel et al., 2003]. The suppressed temporal slopes on these sites are mainly caused by too weak responses of the water isotopes locally in some ice core sites, which is likely caused by the poor simulation in the coarse resolution model for local climate as well as its deficiency in the isotope module in the ice phase. The fact that the model is able to reproduce the spatial slope as in the observation but fails to reproduce the temporal slope locally on some ice core sites suggests that it is much more difficult to simulate the local temporal slope than the large-scale spatial slope, perhaps due to the difficulty for our coarse resolution climate models in capturing some local climate features and the lower model topography height (by about 1 km than the observation over Greenland). Indeed, some models with higher resolutions seem to be able to simulate the temporal slope locally over Greenland and Antarctica stations comparable with the observation [e.g., Lee et al., 2008].

Although our model simulation is inconsistent with some ice core observations locally, it is still possible that the overall temporal slope in the model in each hemisphere resembles that in the real world. If true, our model simulation would still suggest a temporal slope about half of the spatial slope, averagely over each hemisphere. Regardless of the model-data comparison, the reduced temporal slope relative to the spatial slope over most regions is a robust feature in the isoCAM3. Notably, the reduced temporal slope is robust to the changes of the seasonality of precipitation and its weighting to $\delta^{18}\text{O}_w$ and SAT (Figure S2). First, we have recalculated the slopes between the annual mean $\delta^{18}\text{O}_w$ and the precipitation weighted SAT. The average spatial (NH, $0.65‰\text{ }^{\circ}\text{C}^{-1}$; SH, $0.55‰\text{ }^{\circ}\text{C}^{-1}$) and temporal (NH, $0.40‰\text{ }^{\circ}\text{C}^{-1}$; SH, $0.32‰\text{ }^{\circ}\text{C}^{-1}$) slopes both increase slightly, and the temporal slope is still reduced by $\sim 40\%$ from the average spatial slope. Second, the result remains little changed if we use the simple annual mean $\delta^{18}\text{O}_w$ (no precipitation weighting) and the precipitation weighted SAT (as in Werner et al. [2000]). The average spatial slopes are $0.70‰\text{ }^{\circ}\text{C}^{-1}$ and $0.55‰\text{ }^{\circ}\text{C}^{-1}$ for the NH and SH, respectively, and the average temporal slopes are $0.35‰\text{ }^{\circ}\text{C}^{-1}$ and $0.33‰\text{ }^{\circ}\text{C}^{-1}$ for the NH and SH, respectively. Third, we also have recalculated the slopes using the annual mean $\delta^{18}\text{O}_w$ weighted by the precipitation seasonal cycle of the present day (00 ka experiment) for all the snapshots (so the precipitation seasonality weighting remains unchanged across all snapshots), while the SAT is still the simple annual mean.

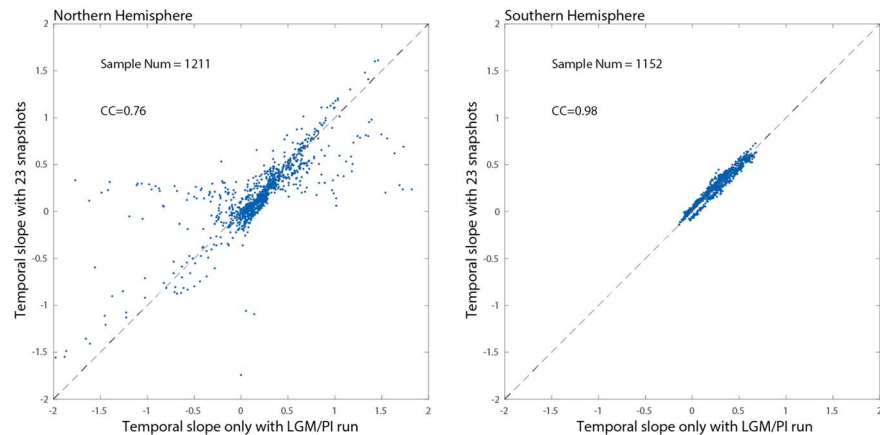


Figure 6. Comparison between the temporal slope from the regression of all the 23 snapshots and that simply from the LGM-present difference at each grid point in the extratropical (left) Northern Hemisphere and (right) Southern Hemisphere. For both hemispheres, only the temporal slopes that pass the significance test are compared.

The average spatial slope is $0.54\text{‰}\text{C}^{-1}$ and $0.52\text{‰}\text{C}^{-1}$ in the NH and SH, respectively, while the temporal slope is $0.32\text{‰}\text{C}^{-1}$ and $0.33\text{‰}\text{C}^{-1}$ for the NH and SH, respectively.

Finally, the model temporal slope also remains stable throughout the deglaciation, similar to the spatial slope discussed in Figure 3. As a result, the temporal slope derived from the regression of the 23 deglaciation snapshots can be approximated reasonably well by that derived from the difference between two time slices only, notably, LGM and the present. This can be seen in Figure 6, which compares the temporal slope from the regression of all the 23 snapshots and that simply from the difference between LGM (22 ka) and present (00 ka) at each model grid point in the Northern (Figure 6, left) and Southern (Figure 6, right) Hemispheres. The two different temporal slopes show very similar spatial pattern with the spatial correlation between the two types of temporal slopes as 0.76 and 0.98 for the Northern and Southern Hemisphere, respectively. The exceptions are the scatters over the region of Greenland-Iceland-Nordic sea (GIN) (not shown), where the regressed temporal slope is ~ 0.3 while the LGM-present temporal slope ranges from -2 to 0 , reflecting perhaps the dramatic climate changes in the GIN region during the deglaciation, especially during abrupt climate change events of Heinrich Statal 1, Bølling-Allerød warming, and Younger Dryas. Overall, however, our model supports previous modeling works, which have all estimated the temporal slope using the LGM-present [e.g., Lee *et al.*, 2008].

4. Mechanisms for the Temporal Slope

Boyle [1997] interpreted the smaller temporal slope than spatial slope between the LGM and the present as caused by the changes in the vapor source temperature (SST) and global isotopic composition associated with ice volume. Here we attempt to further understand the reduced temporal slope following Boyle's mechanism (1997) but using a more comprehensive and quantitative approach. We will maintain the two major assumptions of Boyle's. First, the spatial slope does not change substantially between the LGM and present, a feature that has been confirmed in our model (Figure 3). Second, the water isotope is determined mainly by the Rayleigh distillation process. In the Rayleigh distillation model [Dansgaard, 1964; Gat, 1996], the condensation water isotope $\delta^{18}\text{O}_w$ increases with the condensation temperature T (which is often treated as local surface air temperature approximately (Using temperature above the inversion layer does not change our conclusion significantly in the model)) but decreases with the vapor source temperature T_0 , the latter being mostly SST in the tropics. Therefore, for a specific site of location x at time t , the water isotope change can be related to the change of condensation temperature $T(x, t)$ and source temperature $T_0^*(x, t)$ approximately linearly as [Jouzel *et al.*, 1997]

$$\delta^{18}\text{O}(x, t) = aT(x, t) - bT_0^*(x, t) + d^*(x, t). \quad (1)$$

Here T , T_0^* , and $\delta^{18}\text{O}$ denote the deviation from their reference values T_r , T_{0r} , and $\delta^{18}\text{O}_r$, the last being a function of the former two through the Rayleigh distillation relation. For our realistic climate application, where the reference temperatures are roughly in the range of $\sim 15 - 25^\circ\text{C}$ for source temperature (mostly tropical

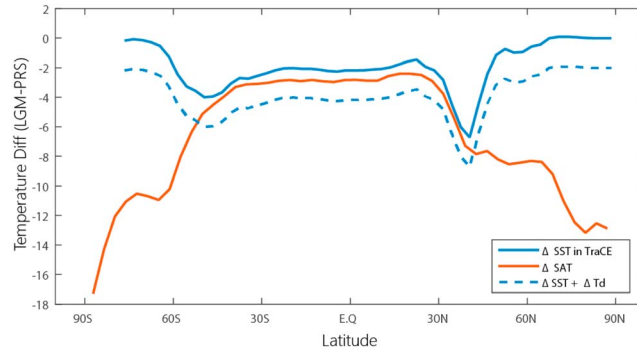


Figure 7. Zonal mean annual cooling of SAT (red solid) and SST (blue solid) between LGM and present. The dash blue line shows the total equivalent source temperature cooling by adding the ice volume effect.

SST) and -30 to 0°C for site temperature (middle- and high-latitude air temperature), Rayleigh distillation gives $a \approx 1.1\text{‰}\text{°C}^{-1}$, $b \approx 0.55\text{‰}\text{°C}^{-1}$. The $d^*(x, t)$ represents the contribution from the processes other than Rayleigh distillation, such as the global isotopic composition [Boyle, 1997] and evaporation recharge [Lee et al., 2008]. We now separate T_0^* and d^* further into the spatially varying part and the regional mean as $T_0^*(x, t) = T_1(x, t) + T_0(t)$ and $d^*(x, t) = d_1(x, t) + d(t)$. The isotope equation can therefore be rewritten as

$$\delta^{18}\text{O}(x, t) = \alpha_S T(x, t) - b T_0(t) + d(t), \quad (2)$$

where, as in Boyle and as in our simulation (Figures 1 and 2), the spatial slope is assumed as $\alpha_S \approx 0.6\text{‰}\text{°C}^{-1}$ and remains unchanged with time, such that the spatial dependence can be combined together in a single term $\alpha T(x, t) - b T_1(x, t) + d_1(x, t) = \alpha_S T(x, t)$. To derive the temporal slope between, say, LGM and present, we first derive from equation (2) the temporal change between two time slices, denoted by Δ , as

$$\Delta \delta^{18}\text{O} = \alpha_S \Delta T - b \Delta T_0 + \Delta d.$$

Divided by the temperature change ΔT on both sides, the temporal slope can be related to the spatial slope as

$$\alpha_T \equiv \frac{\Delta \delta^{18}\text{O}}{\Delta T} = \alpha_S \left(1 - r \frac{\Delta T_0 + \Delta T_d}{\Delta T} \right)$$

or equivalently in the *slope ratio equation*

$$\frac{\alpha_T}{\alpha_S} = 1 - r \frac{\Delta T_0 + \Delta T_d}{\Delta T}. \quad (3)$$

Here $r = b/\alpha_S$. For convenience, the additional effect Δd has been rescaled as an equivalent source temperature change as

$$\Delta T_d = -\frac{\Delta d}{r \alpha_S} \equiv -\frac{\Delta d}{b}. \quad (4)$$

From equation (3), it is clear that the temporal slope is smaller than the spatial slope if

$$0 < r \frac{\Delta T_0 + \Delta T_d}{\Delta T} < 1. \quad (5)$$

Here

$$r = \frac{b}{\alpha_S}. \quad (6)$$

Since Rayleigh distillation gives $b \approx 0.55\text{‰}\text{°C}^{-1}$, empirically we have the constant spatial slope $\alpha_S \approx 0.6\text{‰}\text{°C}^{-1}$. We have semiempirically $r = \frac{b}{\alpha_S} \approx 1$; therefore, the temporal slope will be smaller than the spatial slope as long as the local temperature change is larger than the total (equivalent) source temperature change. Since the source temperature is dominated by the SST at lower latitudes, the larger local temperature response in the middle and high latitudes corresponds to, roughly, the “polar amplification” response. This polar amplification response can be seen clearly in our model between LGM and present, in the zonal mean annual cooling in SAT and SST (Figure 7). Tropical SST cools by about 2°C , with the maximum SST cooling less than 6°C and 4°C in the NH and SH, respectively (blue solid). The ice volume effect is equivalent to a global enrichment of $\Delta d \approx 1.1\text{‰}$ [Duplessy et al., 2002] and in turn an equivalent source temperature cooling of about $\Delta T_d \approx 2^\circ\text{C}$ according to equation (4). This gives a total equivalent source temperature change ΔT_0

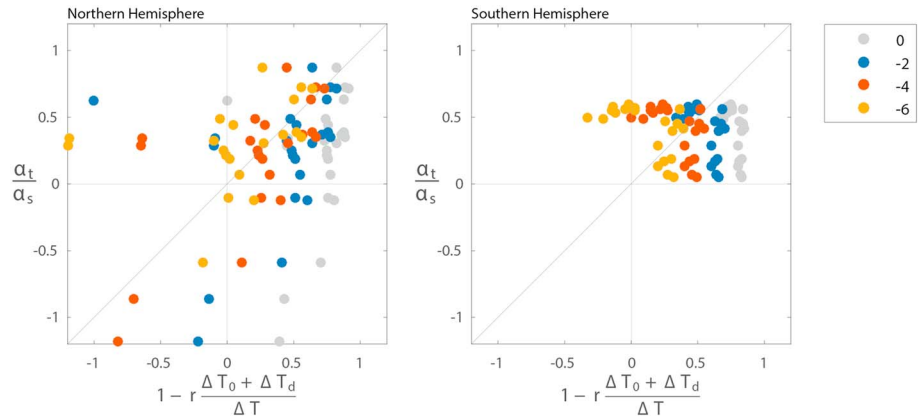


Figure 8. Forward testing of equation (3) by comparing the temporal/spatial slope ratio in the model against the theoretical estimation using equation (3) for all the subregions in the (left) Northern and (right) Southern Hemisphere. The grey, blue, red, and orange markers represent the estimation using a hypothetical source temperature change of $\Delta T_0 = 0^\circ\text{C}$, -2°C , -4°C , and -6°C in equation (3), respectively. Here we use a fixed spatial slope which is $0.6 \text{‰ } ^\circ\text{C}^{-1}$, and the equivalent source temperature cooling caused by ice volume effect is about 2°C .

+ ΔT_d of about 4°C – 7°C (blue dash). In contrast, the SAT cools much more in the extratropics poleward of 40° , more than 8°C and 6°C in the NH and SH, respectively, and can reach over 12°C and 16°C in the NH and SH polar regions. Given that the source is likely dominated by the tropical ocean where the SST change is the smallest, it is obvious that the local temperature change can easily reach twice that of the total equivalent source temperature cooling, leading to a temporal slope about half of the spatial slope, as seen in Figures 2–5. These model SST change and SAT change are largely consistent with the reconstructions [e.g., Annan and Hargreaves, 2013]. Therefore, equation (3) may also be applied to the real world, inferring an overall reduction of temporal slope to about half of the spatial slope in the observation.

The slope ratio equation (3) provides a semiempirical relation for estimating the temporal slope from the responses of the total equivalent source temperature, the local temperature, and the given spatial slope. This equation reflects basically the Boyle mechanism and has employed the major assumptions: Rayleigh distillation and a fixed spatial slope. Compared with the graphic technique of Boyle, however, equation (3) gives a more comprehensive and quantitative representation of the temporal slope, a point to be returned to later regarding Figure 10. It states explicitly that the reduced temporal slope from the spatial slope is the result of the greater change in local temperature than in the (equivalent) source temperature or tropical SST or, approximately, the polar amplification. Since polar amplification is generally a robust characteristic of global climate change, the reduced temporal slope than spatial slope should be generally valid in the real world.

The slope ratio equation (3) can also be used to help understanding the temporal slopes in different regions. First, it should be pointed out that equation (3) can be considered applicable to regional responses, such as a subregion in Figure 2 if the spatial mean ΔT_0 and Δd are considered as averaged for the subregion and therefore may differ across different regions. One implicit limitation, however, is that the exact region for source temperature is unknown for different subregions without additional Lagrangian tracking analysis or sensitivity experiments. Nevertheless, we can test equation (3) with reasonable guesses of the source temperatures in two approaches, a forward approach and a backward approach.

We first test the slope ratio equation (3) in the forward approach by comparing the model temporal/spatial slope ratio against the theoretical value using (3) for four choices of source temperature changes in the range of possible source temperature changes. Figure 8 (left and right) show the temporal/spatial slope ratio in the model (y axis) against the theoretical value in equation (3) (x axis) for the 48 subregions in the NH (Figure 2a) and SH (Figure 2b), respectively. The ratios are marked in grey, blue, red, and orange for $\Delta T_0 = 0^\circ\text{C}$, -2°C , -4°C , and -6°C , respectively. Therefore, each dot is shifted from right to left from grey, to blue, red, and finally orange. Here for simplicity, we have used $r = 1$ and a typical spatial slope $\alpha_s = 0.6 \text{‰ } ^\circ\text{C}^{-1}$, and the result remains similar if the local α_s and the corresponding r are used (not shown). A global enrichment of $\Delta T_d = 2^\circ\text{C}$ is also prescribed for all the cases. It is seen that with the possible source temperature changes, most of the ratios fall into the first quadrant, suggesting a robust estimation of the

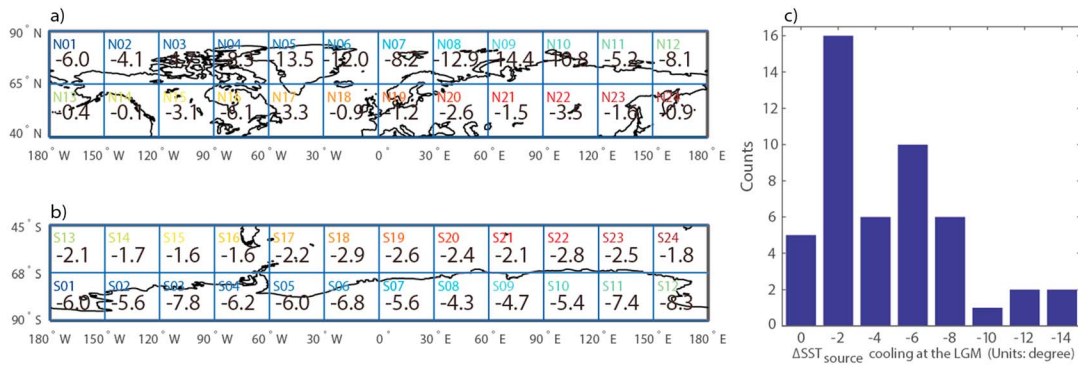


Figure 9. Backward testing of equation (3) by estimating the source temperature cooling at the LGM required by equation (3). (a) Northern Hemisphere, (b) Southern Hemisphere, and (c) the histogram of estimated source temperature cooling.

positive temporal slope of the same sign in the theory (x axis) and model (y axis). Furthermore, many model ratio points are clustered round 0.5, reflecting most regions with a temporal slope about half of the spatial slope as shown in Figures 4 and 5. For some source temperature changes, especially $\Delta T_d = -2^\circ\text{C}$, many ratio points are close to the diagonal line, suggesting a good estimation of the value of the temporal slope using (3). This includes a few points of negative temporal slope (in the third quadrant.) This reflects the small temperature change relative to the source temperature change. For example, as pointed out in Figure 2, in Alaska N01 and N02 regions, the surface temperature exhibits only a slight cooling at the LGM because of the warm air advection steered by the topographic effect of the Cordilleran Ice Sheet [e.g., Lofverstrom *et al.*, 2014]. A too small local cooling, according to equation (3), will lead to a negative temporal slope, because the source temperature change cannot be smaller than the tropical SST change (plus the ice volume effect). In this forward testing, the exact source temperature change is unknown for each region. Yet the good prediction of temporal slope for most regions within reasonable range of source temperature changes suggests that equation (3) is reasonably valid.

We now test the slope ratio equation (3) in the backward approach. Now we assume that equation (3) predicts the model temporal slope/spatial slope ratio for each region perfectly (Figures 4 and 5) and then solve for the required source temperature to see if the source temperature distribution is reasonable. Figures 9a and 9b show the source temperature distributions for the NH and SH, respectively. It is seen that over most subregions in between 40 and 65°, the source temperature change is small, of -1°C to -2°C , implying mainly a source of tropics, as seen from the temperature changes in Figure 7. Further poleward, the source temperature change increases, implying the increased contribution locally from the extratropical SST. Figure 9c further shows the histogram of the required ΔT_0 . It shows that the most likely ΔT_0 are in the range of -2°C to -8°C , consistent with the SST change (Figure 7). In particular, $\Delta T_0 = -2^\circ\text{C}$ is the dominant contribution. This implies, from the temperature change in Figure 7, that the dominant source region lies in the tropics, consistent with our knowledge of the dominant contribution of tropical evaporation to the global hydrology. There are also a small number of regions where the required ΔT_0 is beyond the model SST change. This can be attributed to the inaccuracy of equation (3) as well as the missing effects such as evaporation recharge and land recycling. In our model, however, unlike in Lee *et al.* [2008], the evaporation recharge effect is not significant (not shown). Overall, the backward test also suggests that equation (3) gives a reasonable prediction of the temporal slope. Therefore, the slope ratio equation provides a useful tool for understanding temporal slopes in the model and in the real world.

5. Conclusion

In this study, we investigate the temporal and spatial slopes during the last 21,000 years over the middle and high latitudes by analyzing a series of snapshot simulations of global climate and water isotopes in isoCAM3 with the focus on the three questions raised in section 1. First, our model simulation suggests that both the temporal slope and spatial slope remain largely stable through the last deglaciation. Second, the temporal slope can vary substantially across regions. Nevertheless, on average, and most likely, the temporal slope is around $0.3\% \text{ } ^\circ\text{C}^{-1}$, which is about half of the spatial slope. Finally, the temporal slope can be understood

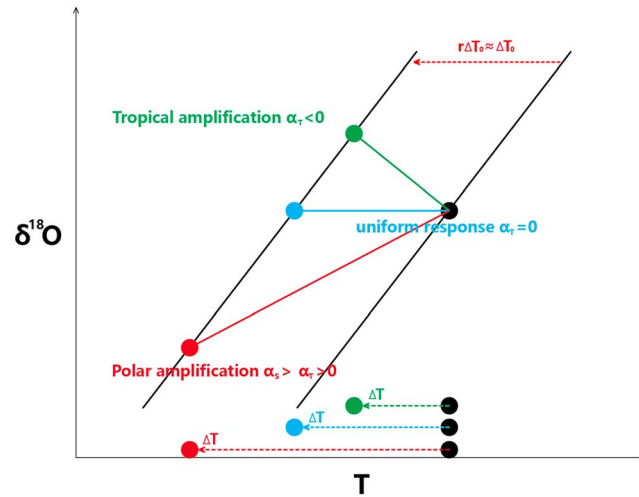


Figure 10. Schematic figure showing how the slope equation quantifies the Boyle mechanism. The spatial slope is assumed unchanged at LGM and 0 ka (black lines). On this figure, the abscissa is the site temperature, the equivalent cooling induced by a colder source temperature is $r\Delta T_0$ (red dash), which approximately equals the source temperature change ΔT_0 because Rayleigh distillation and empirical spatial slope give $b/\alpha_s \approx 1$. If we take the source temperature as the tropical SST, a polar amplification $\Delta T > \Delta T_0$ then leads to a reduced temporal slope relative to the spatial slope (purple line), a uniform response $\Delta T = \Delta T_0$ corresponds to a zero temporal slope (blue line), and a tropical amplification $\Delta T < \Delta T_0$ results in a negative temporal slope (green). The change of site temperature is marked by dashed lines of the corresponding color at the bottom. For simplicity, the figure assumes $\Delta T_d = 0$. An additional enrichment $\Delta T_d > 0$ by other processes such as the ice volume effect and evaporative recharge will always favor a reduced temporal slope (not shown).

With no justification, Boyle seemed to have plotted the ΔT_0 in about the same scale as in T , allowing him to estimate the temporal slope schematically. Our slope equation (2) or (3) suggests that the scale of ΔT_0 should be projected onto the T axis with the scale factor (6) of $r = b/\alpha_s$ as $\left(\frac{b}{\alpha_s}\right)\Delta T_0$. As discussed regarding equation (6), semiempirically, using Rayleigh distillation and observed spatial slope, the scale factor is about 1. Therefore, the shift due to source temperature $\left(\frac{b}{\alpha_s}\right)\Delta T_0$ is approximately the same as the source temperature change itself ΔT_0 . This provides a justification for Boyle's plot and a more quantitative way to estimate the temporal slope. If the change of local temperature is larger than the source temperature change (mainly, tropical SST), as in general true for middle and high latitudes as the polar amplification response, the temporal slope will be reduced from the spatial slope (purple lines, Figure 10). If the local temperature change happens to be comparable with the source temperature in a uniform response, the temporal slope will be further reduced to zero (blue lines, Figure 10). If, furthermore, local temperature change is smaller than the source temperature change or a tropical amplification, the temporal slope becomes negative (green lines, Figure 10). A further enrichment by other processes, such as ice volume and evaporative recharge, $\Delta T_d > 0$, will always favor a reduced temporal slope.

It should be noted that the slope equation (3) assumes a constant spatial slope with time. This assumption is well satisfied in most regions in the extratropics in our iCAM3 simulations, as shown in Figure S3. But, in the small polar region, our model seems to show an increasing trend of spatial slope (increasing from 0.5 at LGM to $0.7\text{‰}\text{°C}^{-1}$ at the present in the Arctic). This change of spatial slope, which can be impacted by local seasonality of precipitation, cloud properties [Jouzel and Merlivat, 1984], and the slope of Rayleigh distillation [Kindler et al., 2014], may also have an impact on the estimation of the temporal slope locally over those regions.

Our work has several limitations. First, our slope equation is far from a full understanding of the slope problem. Indeed, our slope equation only provides a diagnostic relationship between the spatial and temporal

using a semiempirical and semianalytical slope ratio equation (3), which is based on a fixed spatial slope and Rayleigh distillation. The slope equation provides a quantitative framework for the Boyle's mechanism. The slope equation suggests that because the change in local temperature in the middle and high latitudes is usually greater than that of the total equivalent source temperature, predominantly tropical SST, the temporal slope is usually smaller than the spatial slope in the model and, likely, also in the real world.

The quantification of the slope equation on Boyle mechanism can be illustrated schematically in Figure 10. Boyle showed a schematic diagram [Boyle, 1997, Figure 2] with the x axis for site temperature T and y axes for water isotope $\delta^{18}\text{O}_w$. There is one key uncertainty that is not discussed in his illustration: it is the scale of the source temperature change ΔT_0 as projected onto the x axis that is scaled for site temperature T . Without a quantitative scale in the shift in ΔT_0 , one cannot estimate the temporal slope quantitatively, even for a given site temperature change ΔT .

slopes. A full understanding of the spatial and temporal slopes would require a solution of both the spatial and temporal slopes explicitly. Nevertheless, our slope equation can be used as a useful first step toward a quantitative understanding of the water isotope slopes.

Second, one major limitation of our work is the deficient model simulation of the deglaciation $\delta^{18}\text{O}$ evolution locally over Greenland and Antarctica as compared with ice core reconstructions. This may be attributed partly to our model physics. Locally over Greenland, a comparison of the model and GNIP observations (station Thule, Groennedal, Nord, Danmarkshavn, Scoresbysund, Prins Christians sund, and Godthab, Figure S1) shows that the model is able to simulate the seasonal cycle of temperature and precipitation $\delta^{18}\text{O}_w$ consistent with the observation, all peaking in the summer, although the annual mean temperature tends to be colder and the $\delta^{18}\text{O}_w$ tends to be more depleted in the model. However, precipitation is less well simulated. Notably, in the two stations that show a winter peak in precipitation (Nord and Danmarkshavn, Figure S1), the model precipitation peak is shifted to the autumn. This model deficiency may be caused, partly, by the coarse resolution model here. For one thing, our model Greenland topography is biased shallower than in the observations by about 1 km, which could affect water isotopes via the so-called altitude effect. The model water isotope module may also have uncertainties, especially in the cloud ice phase. These model deficiencies can be caused by the deficiencies in model physics, water isotopes, and the coarse resolution. Clearly, improved models are needed in the future for further understanding of the spatial and temporal slopes. At this stage, nevertheless, we believe that our model results are relevant to the real world in general, because our model is able to simulate many major features of the present-day climate and water isotopes over most regions [e.g., Wen et al., 2016], including the spatial slope and some interannual temporal slopes. The slope ratio equation (3) therefore provides a potentially useful tool to understand and assess the temporal slopes in climate models and the real world in the future.

Acknowledgments

This work is supported by National Science Foundation of China (grants 41130105, 41130962, and 41005035), China Scholarship Council, and NSF C2P2 and DOE SciDac. The GNIP data can be accessed online (<http://www.univie.ac.at/cartography/project2/wiser/index.php>). The output of the isoCAM3 experiments can be obtained by sending a written request to the corresponding authors (Jian Guan, lotusescy@pku.edu.cn, and Zhengyu Liu, zliu3@wisc.edu).

References

- Annan, J. D., and J. C. Hargreaves (2013), A new global reconstruction of temperature changes at the Last Glacial Maximum, *Clim. Past*, *9*, 367–376.
- Boyle, E. A. (1997), Cool tropical temperatures shift the global $\delta^{18}\text{O}$ -T relationship: An explanation for the ice core $\delta^{18}\text{O}$ -borehole thermometry conflict?, *Geophys. Res. Lett.*, *24*, 273–276, doi:10.1029/97GL00081.
- Buizert, C., et al. (2014), Greenland temperature response to climate forcing during the last deglaciation, *Science*, *345*, 1177–1180.
- Craig, H. (1961), Standard for reporting concentrations of deuterium and oxygen-18 in natural waters, *Science*, *133*, 1833–1834.
- Cuffey, K. M., R. B. Alley, P. M. Grootes, J. M. Bolzan, and S. Anandakrishnan (1994), Calibration of the $\delta^{18}\text{O}$ isotopic paleothermometer for central Greenland, using borehole temperatures, *J. Glaciol.*, *40*, 341–349.
- Cuffey, K. M., G. D. Clow, R. B. Alley, M. Stuiver, E. D. Waddington, and R. W. Saltus (1995), Large arctic temperature change at the Wisconsin-Holocene glacial transition, *Science*, *270*, 455–458.
- Dansgaard, W. (1964), Stable isotopes in precipitation, *Tellus*, *16*, 436–468.
- Duplessy, J.-C., L. Labeyrie, and C. Waelbroeck (2002), Constraints on the ocean oxygen isotopic enrichment between the Last Glacial Maximum and the Holocene: Paleoclimatological implications, *Quat. Sci. Rev.*, *21*(1–3), 315–330, doi:10.1016/S0277-3791(01)00107-X.
- Gat, J. R. (1996), Oxygen and hydrogen isotopes in the hydrological cycle, *Annu. Rev. Earth Planet. Sci.*, *24*, 225–262.
- Grootes, P. M., M. Stuiver, J. W. C. White, S. Johnsen, and J. Jouzel (1993), Comparison of oxygen isotope records from the GISP2 and GRIP Greenland ice cores, *Nature*, *366*(6455), 552–554, doi:10.1038/366552a0.
- Hendricks, M. B., D. J. DePaolo, and R. C. Cohen (2000), Space and time variation of $\delta^{18}\text{O}$ and δD in precipitation: Can paleotemperature be estimated from ice cores?, *Global Biogeochem. Cycles*, *14*, 851–861, doi:10.1029/1999GB001198.
- Johnsen, S. J., D. Dahl-Jensen, W. Dansgaard, and N. S. Gundestrup (1995), Greenland temperatures derived from GRIP bore hole temperature and ice core isotope profiles, *Tellus, Ser. B*, *47*, 624–629.
- Johnsen, S. J., et al. (1997) The $\delta^{18}\text{O}$ record along the Greenland Ice Core Project deep ice core and the problem of possible Eemian climatic instability, *J. Geophys. Res.*, *102*(C12), 26,397–26,410.
- Jouzel, J., and L. Merlivat (1984), Deuterium and oxygen 18 in precipitation: Modeling of the isotopic effects during snow formation, *J. Geophys. Res.*, *89*, 11,749–11,757, doi:10.1029/JD089iD07p11749.
- Jouzel, J., et al (1997), Validity of the temperature reconstruction from water isotopes in ice cores, *J. Geophys. Res.*, *102*, 26,471–26,487.
- Jouzel, J., F. Vimeux, N. Caillon, G. Delaygue, G. Hoffmann, V. Masson-Delmotte, and F. Parrenin (2003), Magnitude of isotope/temperature scaling for interpretation of central Antarctic ice cores, *J. Geophys. Res.*, *108*(D12), 4361, doi:10.1029/2002JD002677.
- Kindler, P., M. Guillevic, M. Baumgartner, J. Schwander, A. Landais, and M. Leuenberger (2014), Temperature reconstruction from 10 to 120 kyr b2k from the NGRIP ice core, *Clim. Past*, *10*, 887–902, doi:10.5194/cp-10-887-2014.
- Krinner, G., C. Genthon, and J. Jouzel (1997), GCM analysis of local influences on ice core δ signals, *Geophys. Res. Lett.*, *24*, 2825–2828, doi:10.1029/97GL52891.
- Lee, J.-E., I. Fung, D. J. DePaolo, and C. C. Henning (2007), Analysis of the global distribution of water isotopes using the NCAR atmospheric general circulation model, *J. Geophys. Res.*, *112*, D16306, doi:10.1029/2006JD007657.
- Lee, J.-E., I. Fung, D. J. DePaolo, and B. Otto-Bliesner (2008), Water isotopes during the Last Glacial Maximum: New general circulation model calculations, *J. Geophys. Res.*, *113*, D19109, doi:10.1029/2008JD009859.
- Liu, Z., et al. (2009), Transient simulation of last deglaciation with a new mechanism for Bølling-Allerød warming, *Science*, *325*, 310–314.
- Liu, Z., et al. (2012), Younger Dryas cooling and the Greenland climate response to CO_2 , *Proc. Natl. Acad. Sci. U.S.A.*, *109*, 11,101–4, doi:10.1073/pnas.1202183109.

- Liu, Z., et al. (2014), Chinese cave records and the East Asia summer monsoon, *Quat. Sci. Rev.*, *83*, 115–128, doi:10.1016/j.quascirev.2013.10.021.
- Lofverstrom, M., R. Caballero, J. Nilsson, and J. Kleman (2014), Evolution of the large-scale atmospheric circulation in response to changing ice sheets over the last glacial cycle, *Clim. Past Discuss.*, *10*, 1381–1420.
- Noone, D., and C. Sturm (2010), Comprehensive dynamical models of global and regional water isotope distributions, in *Isoscapes: Understanding Movement, Patterns, and Process on Earth Through Isotope Mapping*, edited by J. B. West et al., pp. 195–219, Springer, Dordrecht, Netherlands.
- Salamatin, A. N., V. Y. Lipenkov, N. I. Barkov, J. Jouzel, J. R. Petit, and D. Raynaud (1998), Ice core age dating and paleothermometer calibration based on isotope and temperature profiles from deep boreholes at Vostok Station (East Antarctica), *J. Geophys. Res.*, *103*, 8963–8977, doi:10.1029/97JD02253.
- Schrag, D. P., G. Hampt, and D. W. Murray (1996), Pore fluid constraints on the temperature and oxygen isotopic composition of the glacial ocean, *Science*, *272*, 1930–1932.
- Shuman, C., D. Bromwich, J. Kipfstuhl, and M. Schwager (2001), Multiyear accumulation and temperature history near the North Greenland Ice Core Project site, north central Greenland, *J. Geophys. Res.*, *106*, 33,853–33,866, doi:10.1029/2001JD900197.
- Sodemann, H., V. Masson-Delmotte, C. Schwierz, B. M. Vinther, and H. Wernli (2008), Interannual variability of Greenland winter precipitation sources: 2. Effects of North Atlantic Oscillation variability on stable isotopes in precipitation, *J. Geophys. Res.*, *113*, D12111, doi:10.1029/2007JD009416.
- Wen, X., Z. Liu, Z. Chen, E. Brady, D. Noone, Q. Zhu, and J. Guan (2016), Modeling precipitation $\delta^{18}\text{O}$ variability in East Asia since the Last Glacial Maximum: Temperature and amount effects across different time scales, *Clim. Past Discuss.*, doi:10.5194/cp-2016-2, in press.
- Werner, M., U. Mikolajewicz, M. Heimann, and G. Hoffmann (2000), Borehole versus isotope temperatures on Greenland: Seasonality does matter, *Geophys. Res. Lett.*, *27*, 723–726, doi:10.1029/1999GL006075.
- Werner, M., M. Heimann, and G. Hoffmann (2001), Isotopic composition and origin of polar precipitation in present and glacial climate simulations, *Tellus, Ser. B*, *53*, 53–71.